Supplement of Atmos. Chem. Phys., 26, 13557–13579, 2026
https://doi.org/10.5194/acp-26-13557-2026-supplement

Atmospheric Chemistry and Physics
Open Access

Supplement of

Simulated reductions in heterogeneous isoprene epoxydiol reactive uptake from aerosol morphology in the contiguous United States using the Community Multiscale Air Quality Model (CMAQv5.3.2)

Sara L. Farrell et al.

Correspondence to: Sara L. Farrell (slfarrel@live.unc.edu) and William Vizuete (vizuete@unc.edu)

Table S1. For the saprctic07_ae7i chemical mechanism the aerosol species names, descriptions, anthropogenic (anth) or biogenic (biog) source, organic matter to organic carbon ratios ($OM:OC$) (Pye et al., 2017), atomic oxygen-to-carbon ratios ($O:C$) (Pye et al., 2017), molar mass (M) (Pye et al., 2017), saturation concentrations (C^0), hygroscopicity coefficients (k_{org}) (Petters et al., 2007), and predicted glass transition temperatures (T_g) with each parameterization (Li et al., 2020; Shiraiwa et al., 2017; Zhang et al., 2019b) found in Table 1.

Species Name	**Description**	**Source**	$\boldsymbol{OM:OC}$	$\boldsymbol{O:C}$	$\boldsymbol{M}$ **(gmol^{-1})**	**C^0 (μg m^{-3})**	$\boldsymbol{k_{org}}$	**Predicted T_g (K) Shiraiwa**	**Predicted T_g (K) Zhang @ 298**	**Predicted T_g (K) Li**
AAVB1	low volatility organic particulate matter from oxidation of anthropogenic VOCs (benzene, toluene, xylene, PAHs, alkanes)	anth	2.72	1.20	198.00	0.01	0.20	309.04	301.27	313.19
AAVB2	semivolatile organic particulate matter from oxidation of anthropogenic VOCs (benzene, toluene, xylene, PAHs, alkanes)	anth	2.27	1.10	179.00	1.00	0.15	289.57	264.55	289.10
AAVB3	semivolatile organic particulate matter from oxidation of anthropogenic VOCs (benzene, toluene, xylene, PAHs, alkanes)	anth	2.18	0.90	169.00	10.00	0.14	265.30	243.10	275.22
AAVB4	semivolatile organic particulate matter from oxidation of anthropogenic VOCs (benzene, toluene, xylene, PAHs, alkanes)	anth	2.00	0.60	158.00	100.00	0.12	229.71	219.46	258.82
ADIM	2-methyltetrol/methyltetrol sulfate dimer	biog	2.07	0.74	248.23	0.0007	0.13	299.78	320.19	330.77

AGLY	Glyoxal / methylglyoxal SOA	biog	2.13	0.77	66.40	0.046	0.13	159.67	281.87	307.37
AIEOS	IEPOX-derived methyltetrol sulfate	biog	3.60	1.98	216.20	0.004	0.30	378.25	308.15	311.71
AIETET	2-methyltetrol	biog	2.27	0.88	136.15	0.46	0.15	238.65	268.74	293.59
AIMGA	2-methylglyceric acid	biog	2.50	1.10	120.10	22	0.18	247.08	232.08	271.21
AIMOS	methacrolein epoxide derived organosulfate	biog	4.17	2.40	200.16	0.056	0.36	408.04	288.77	299.57
AISO1	SV SOA product from isoprene	biog	2.20	0.81	132.00	116.01	0.14	228.04	216.02	259.22

AISO2	SV SOA product from isoprene	biog	2.23	0.85	133.00	0.62	0.15	232.68	266.15	291.97
AISOPNN	ISOP + NO3 organic nitrates	biog	3.80	2.12	226.00	8.65	0.32	391.74	247.22	279.80
AIVPO1	Intermediate Volatility Primary organic compounds	anth	1.17	0.01	266.00	1000.00	0.03	260.59	200.34	237.11
ALVOO1	LV Oxidized combustion organic compounds	anth	2.27	0.88	136.00	0.01	0.15	238.53	298.62	315.22
ALVOO2	LV Oxidized combustion organic compounds	anth	2.06	0.74	136.00	0.10	0.13	224.36	281.33	302.92
ALVPO1	LV Primary organic compounds	anth	1.39	0.16	218.00	0.10	0.05	238.94	285.02	304.80

AMT1	low volatility particulate matter from monoterpene photoxidation (OH and O3 reaction)	biog	1.63	0.38	300.00	0.01	0.08	299.62	304.15	318.51
AMT2	low volatility particulate matter from monoterpene photoxidation (OH and O3 reaction)	biog	1.63	0.38	200.00	0.10	0.08	243.02	284.36	304.10
AMT3	semivolatile particulate matter from monoterpene photoxidation (OH and O3 reaction)	biog	1.72	0.45	186.00	1.00	0.09	238.55	264.88	289.10
AMT4	semivolatile particulate matter from monoterpene photoxidation (OH and O3 reaction)	biog	1.54	0.30	184.00	10.00	0.07	224.59	243.91	273.29
AMT5	semivolatile particulate matter from monoterpene photoxidation (OH and O3 reaction)	biog	1.54	0.30	170.00	100.00	0.07	212.94	220.22	256.90
AMT6	semivolatile particulate matter from monoterpene photoxidation (OH and O3 reaction)	biog	1.36	0.16	168.00	1000.00	0.05	198.22	195.24	238.52

AMTHYD	organic pseudo-hydrolysis accretion product from monoterpene organic nitrates (AMTNO3J)	biog	1.54	0.30	186.00	53.23	0.07	226.20	227.80	261.58
AMTNO3	semivolatile organic nitrates from monoterpene oxidation	biog	1.90	0.59	231.00	12.00	0.11	280.27	244.34	273.03
AOLGA	Oligomer products of anthropogenic SOA compounds	anth	2.50	1.07	206.00	7.61	0.18	302.58	247.55	277.37
AOLGB	Oligomer products of biogenic SOA compounds	biog	2.10	0.74	248.00	2.63	0.13	299.67	258.95	283.13
AORGC	Cloud-formed SOA	biog	2.00	0.67	177.00	0.003	0.12	250.54	308.65	323.39
APCSO	Potential combustion SOA	anth	2.00	0.67	170.00	0.00001	0.12	245.27	341.74	353.58

APNCOM	Primary Combustion Non-carbon Organic Matter	anth	n/a	n/a	220.00	0.01	0.00	n/a	302.01	n/a
APOC	Primary Combustion Organic Carbon	anth	n/a	n/a	220.00	0.01	0.00	n/a	302.01	n/a
ASQT	SV SOA from sesquiterpenes	biog	1.52	0.30	273.00	24.98	0.07	283.10	238.91	266.84
ASVOO1	SV Oxidized combustion organic products	anth	1.88	0.59	135.00	85000.00	0.11	208.59	140.37	210.06
ASVOO2	SV Oxidized combustion organic products	anth	1.73	0.45	135.00	74000.00	0.09	195.09	142.06	208.94
ASVOO3	SV Oxidized combustion organic products	anth	1.60	0.38	134.00	63000.00	0.08	187.03	143.92	209.06

ASVPO1	SV primary organic compounds	anth	1.32	0.16	230.00	85000.00	0.05	247.44	146.84	203.23
ASVPO2	SV primary organic compounds	anth	1.26	0.08	241.00	74000.00	0.04	249.64	203.22	203.22
ASVPO3	SV primary organic compounds	anth	1.21	0.01	253.00	63000.00	0.03	252.47	203.42	203.42

Table S2. The CMAQ species, noting if said species is lumped (L) or explicitly defined (E), their molecular formula, a suggested surrogate structure, their Simplified Molecular Input Line Entry System (SMILES) structure code, CMAQ molecular weights (M), and the OPEn structure–activity/property Relationship App (OPERA) estimated saturation concentration (C^0) values used for the Zhang and Li parameterizations. Cells in this table labeled N/A have values that already existed in the literature.

CMAQ Species (Explicit/Lumped)	Molecular Formula CMAQ	Surrogate Chemical Structure	SMILES Structure	CMAQ M (g mol^{-1})	OPERA C^0 (μg m^{-3}) (with CMAQ M)
ADIM (L)	C10H16O7	(Pye et al., 2018) 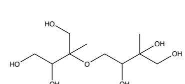 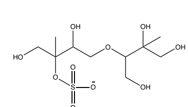	OCC(O)(C)C(O)COC(CO)(C)C(O)CO CC(O)(CO)C(CO)OCC(O)C(C)(CO)OS(=O)(=O)[O-]	248.2	0.0007

AORGC (L)	C7H13O5	(Loeffler et al., 2006) 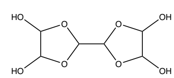	OC2OC(C1OC(O)C(O)O1)OC2O	177	0.003
AIEOS (E)	C5H12O7S	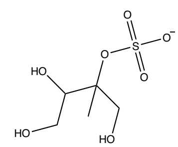	CC(CO)(OS(=O)(=O)[O-])C(O)CO	216.2	0.004
AIETET (E)	C5H12O4	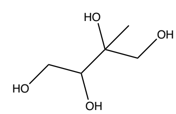	CC(O)(CO)C(O)CO	136.2	0.046
AIMGA (E)	C4H8O4	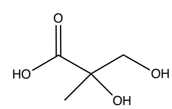	CC(O)(CO)C(=O)O	120.1	(Pye et al., 2018) 22
AIMOS (E)	C4H8O7S	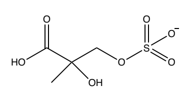	CC(O)(COS(=O)(=O)[O-])C(=O)O	200.2	0.056
AISOPNN (E)	C5H10O8N2	(Rollins et al., 2009) 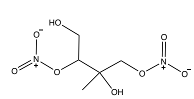	CC(O)(CON(=O)=O)C(CO)ON(=O)=O	226	8.65
AMTHYD (E)	C10H18O3	(Boyd et al., 2015)	CC1(C)C2CCC(CO)(OO)C1C2	186	52.23

		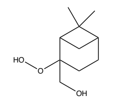			
AOLGA (L)	C7H10O7	N/A	N/A	206	(Pye et al., 2012) 7.61
AOLGB (L)	C10H16O7	N/A	N/A	248	(Sakulyanontvittaya et al., 2008) 2.627
AGLY (L)	C3O2 (-6 Hydrogens)	N/A	N/A	66.4	(Paciga et al., 2014) 0.046
APOC/APNCOM (L)	N/A	N/A	N/A	220	(Simon et al., 2012) 0.01

Table S3. Individual third-order rate constants, $k_{i,j}$, for individual acid-catalyzed and nucleophilic addition reactions that produce IEPOX-SOA constituents (i.e., AIETET, AIEOS, and ADIM) per the saprc07tic_ae7i mechanism (Pye et al., 2017).

$k_{i,j}$	Value ($M^{-2}\ s^{-1}$)	Acid	Nucleophile	Product	Reference
k_{H^+,H_2O}	9×10^{-4}	H^+	H_2O	AIETET	(Eddingsaas et al., 2010; Pye et al., 2017; Pye et al., 2013)
$k_{H^+,SO_4^{2-}}$	1.27×10^{-3}	H^+	SO_4^{2-}	AIEOS	(Budisulistiorini et al., 2017; Riedel et al., 2016)

$k_{H^+,AIEOS}$	2×10^{-4}	H^+	AIEOS	ADIM	(Eddingsaas et al., 2010; Pye et al., 2017; Pye et al., 2013)
$k_{H^+,AIETET}$	2×10^{-4}	H^+	AIETET	ADIM	(Eddingsaas et al., 2010; Pye et al., 2017; Pye et al., 2013)
$k_{HSO_4^-,H_2O}$	1.31×10^{-5}	HSO_4^-	H_2O	AIETET	(Eddingsaas et al., 2010; Pye et al., 2017; Pye et al., 2013)
$k_{HSO_4^-,SO_4^{2-}}$	2.92×10^{-6}	HSO_4^-	SO_4^{2-}	AIEOS	(Eddingsaas et al., 2010; Pye et al., 2017; Pye et al., 2013)
$k_{HSO_4^-,AIEOS}$	2.92×10^{-6}	HSO_4^-	AIEOS	ADIM	(Eddingsaas et al., 2010; Pye et al., 2017; Pye et al., 2013)
$k_{HSO_4^-,AIETET}$	2.92×10^{-6}	HSO_4^-	AIETET	ADIM	(Eddingsaas et al., 2010; Pye et al., 2017; Pye et al., 2013)

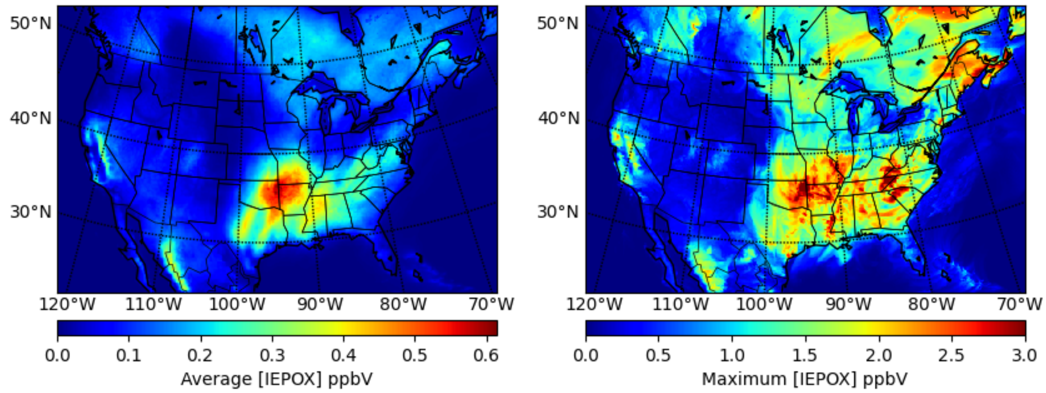

Figure S1. Episode Averaged and Maximum IEPOX concentrations for the SOAS 2013 Field Campaign

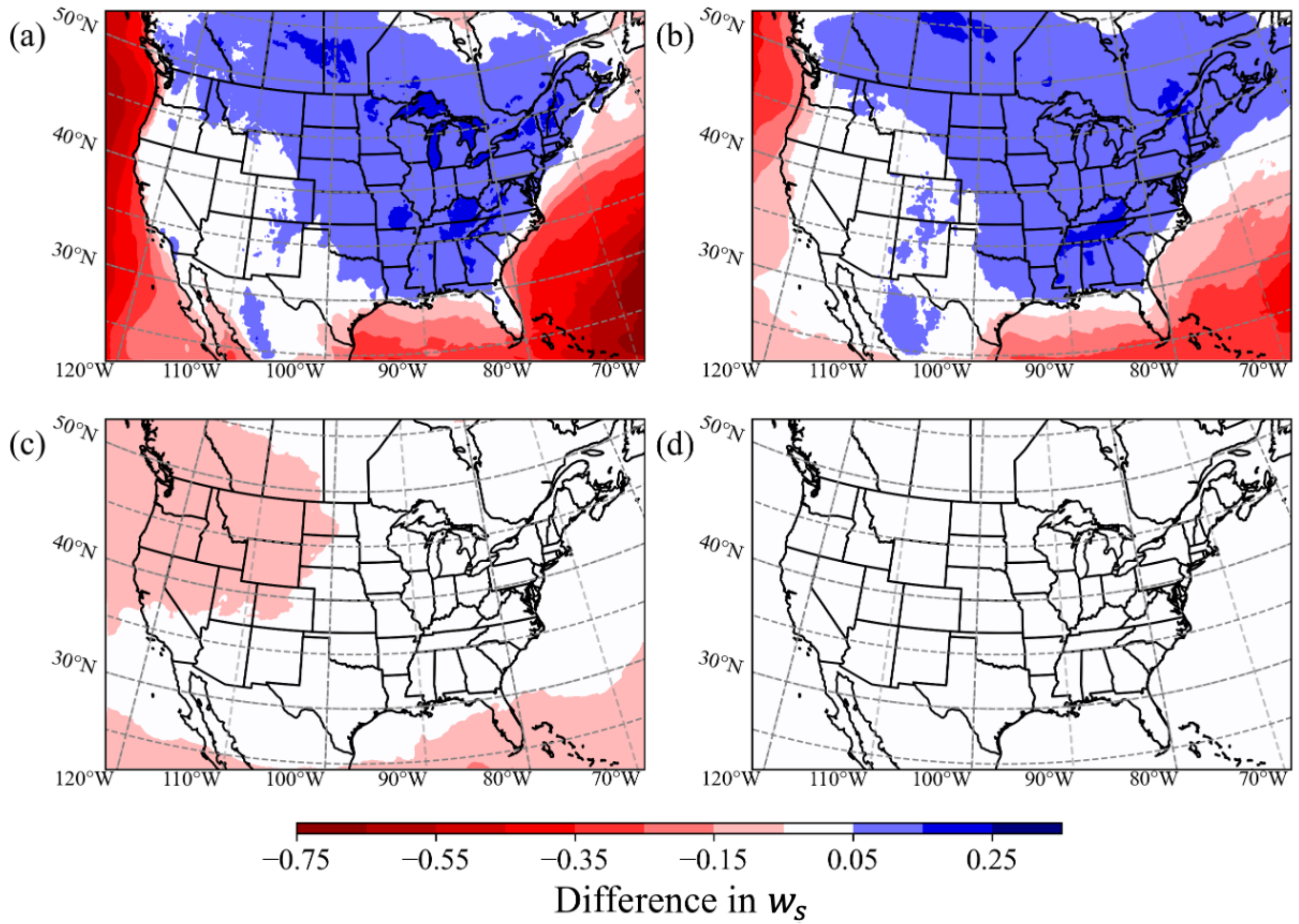

Figure S2. Difference in w_s predicted in the study in comparison to those predicted by Schmedding et al., 2020 and in this study for the entirety of the 2013 SOAS Field Campaign (June 1st – July 31st, 2013) for the surface layer; 1-0.9975 atm (a), layer 18 (corresponding to ~1.8km; 0.82-0.8 atm (b)), layer 28 (corresponding to ~8km; 0.4-0.35 atm (c)), and layer 35 (corresponding to ~17km; 0.05-0 atm (d)). The difference expressed is unitless as w_s is a fraction.

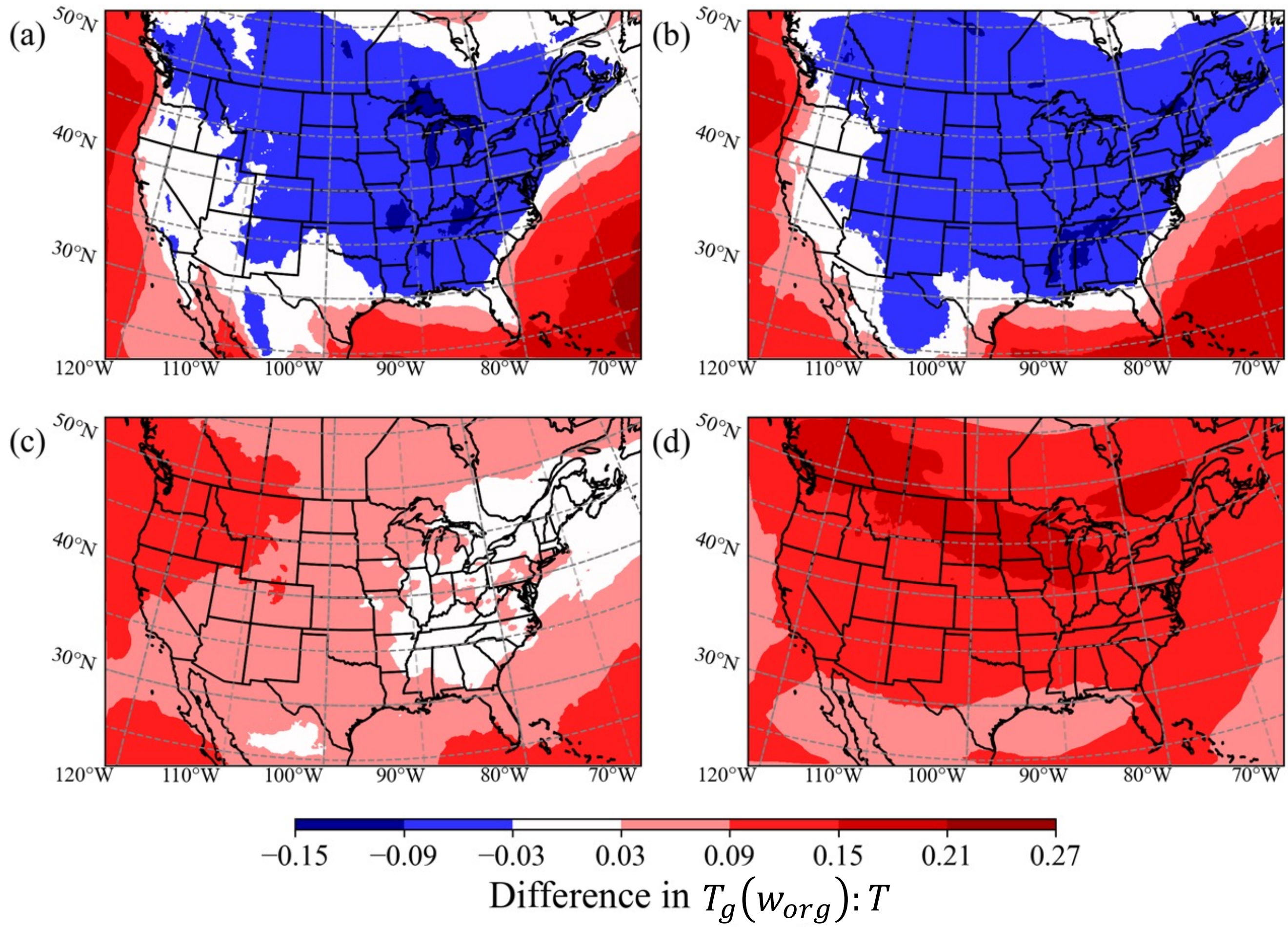

Figure S3. Difference in $T_g(w_{org})$: T predicted in the study in comparison to those predicted by Schmedding et al., 2020 and in this study for the entirety of the 2013 SOAS Field Campaign (June 1st – July 31st, 2013) for the surface layer; 1-0.9975 atm (a), layer 18 (corresponding to ~1.8km; 0.82-0.8 atm (b)), layer 28 (corresponding to ~8km; 0.4-0.35 atm (c)), and layer 35 (corresponding to ~17km; 0.05-0 atm (d)). The difference expressed is unitless as $T_g(w_{org})$: T is a fraction.

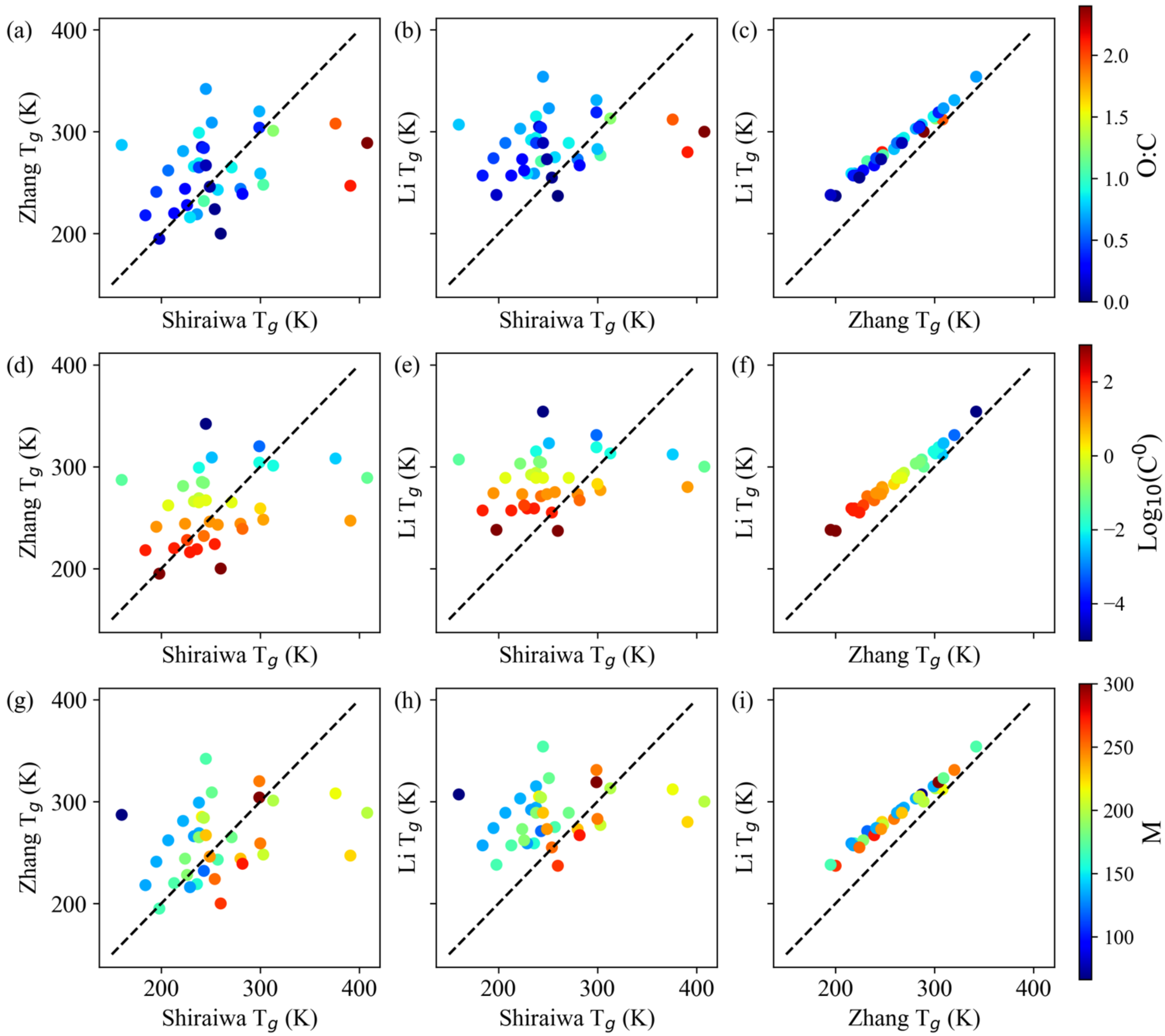

Figure S4. Comparison of T_g between the Shiraiwa and Zhang equations (a, d, and g) the Shiraiwa and Li equations (b, e, and h) and the Zhang and Li equations (c, f, and i) colored by O:C (a-c), volatility (d-f) and molecular weight (g-i).

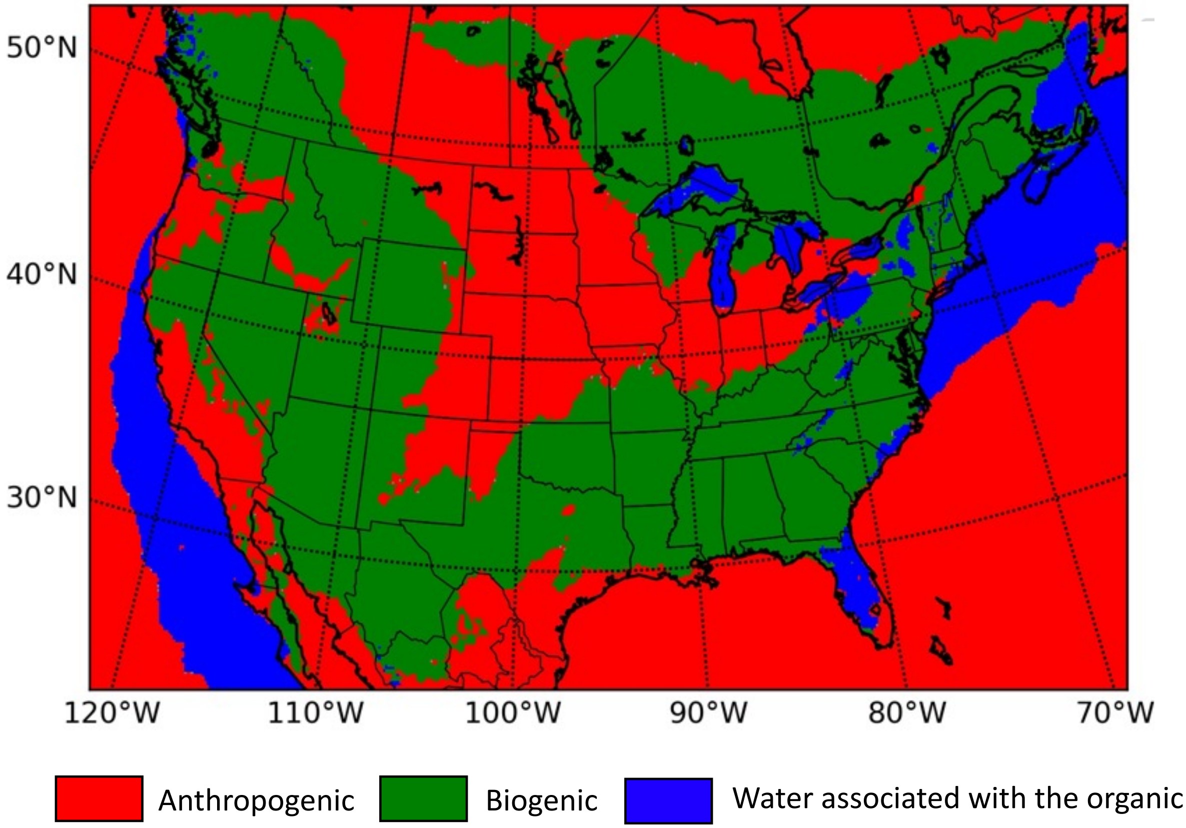

Figure S5. Leading organic aerosol source to total organic aerosol shell mass.

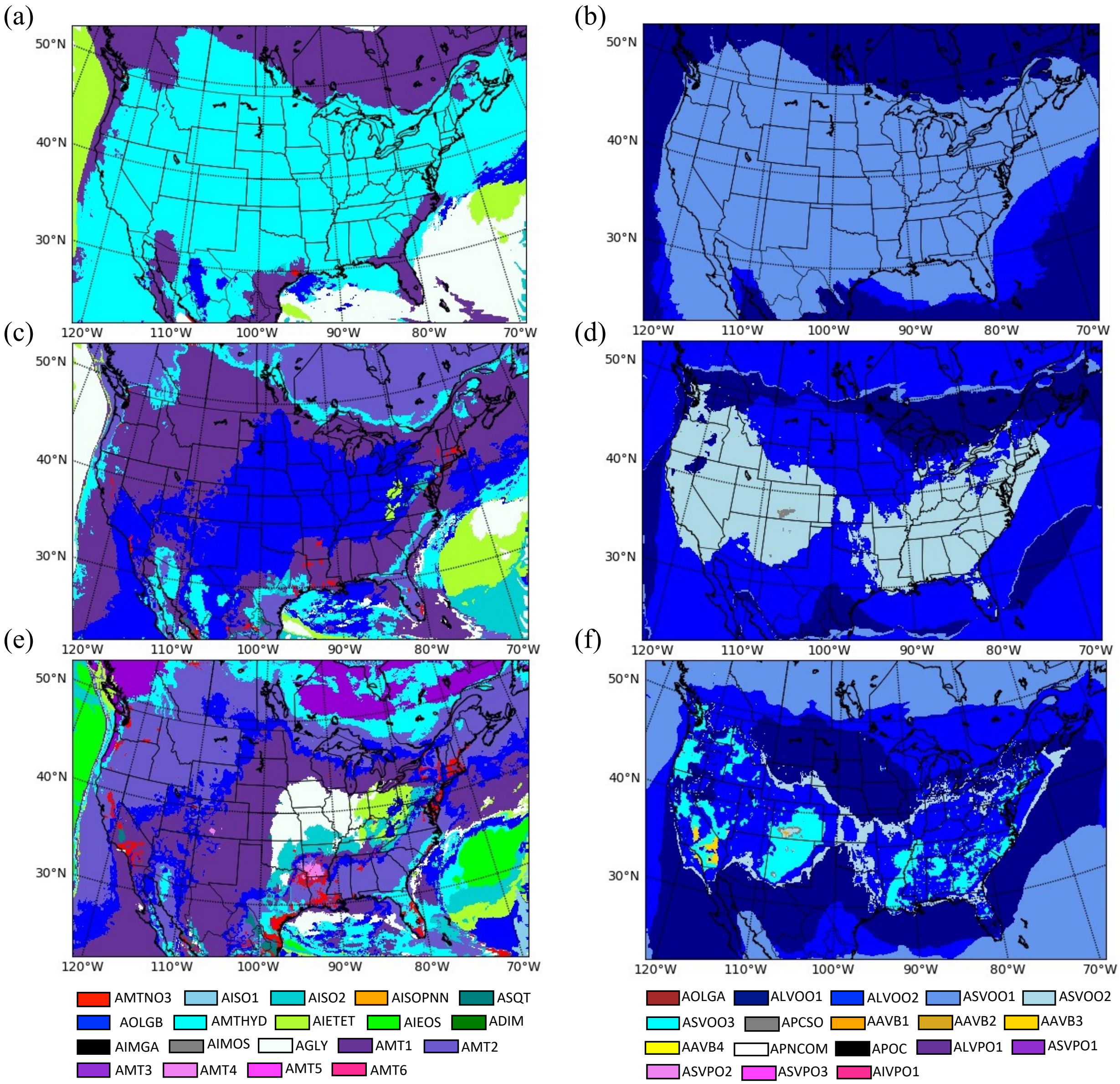

Figure S6. The leading (a-b), second leading (c-d), and third leading (e-f) median aerosol concentration for each grid cell and across the simulation period of either total (a, c, & e) biogenic and (b, d, & f) anthropogenic species. Species names found in Table S1.

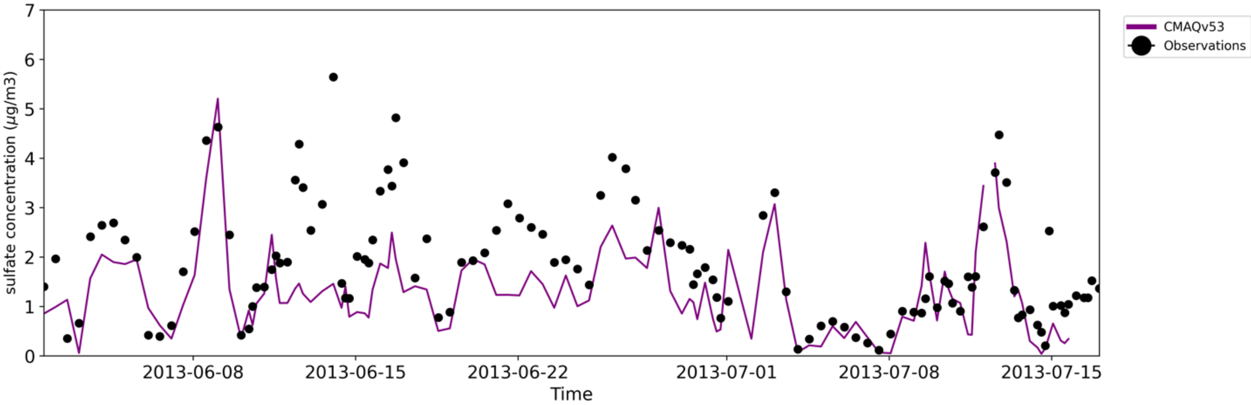

Figure S7. Modeled and observed sulfate concentrations at the LRK SOAS site from June 1st to July 15th 2013.

References

Boyd, C. M., Sanchez, J., Xu, L., Eugene, A. J., Nah, T., Tuet, W. Y., Guzman, M. I., and Ng, N. L.: Secondary organic aerosol formation from the β-pinene+NO₃ system: effect of humidity and peroxy radical fate, Atmos. Chem. Phys., 15(13), 7497-7522, doi:10.5194/acp-15-7497-2015, 2015.

Budisulistiorini, S. H., Nenes, A., Carlton, A. G., Surratt, J. D., McNeill, V. F., and Pye, H. O. T.: Simulating Aqueous-Phase Isoprene-Epoxydiol (IEPOX) Secondary Organic Aerosol Production During the 2013 Southern Oxidant and Aerosol Study (SOAS), Environmental Science & Technology, 51(9), 5026-5034, doi:10.1021/acs.est.6b05750, 2017.

Eddingsaas, N. C., VanderVelde, D. G., and Wennberg, P. O.: Kinetics and products of the acid-catalyzed ring-opening of atmospherically relevant butyl epoxy alcohols, J Phys Chem A, 114(31), 8106-8113, doi:10.1021/jp103907c, 2010.

Li, Y., Day, D. A., Stark, H., Jimenez, J. L., and Shiraiwa, M.: Predictions of the glass transition temperature and viscosity of organic aerosols from volatility distributions, Atmos. Chem. Phys., 20(13), 8103-8122, doi:10.5194/acp-20-8103-2020, 2020.

Loeffler, K. W., Koehler, C. A., Paul, N. M., and De Haan, D. O.: Oligomer Formation in Evaporating Aqueous Glyoxal and Methyl Glyoxal Solutions, Environmental Science & Technology, 40(20), 6318-6323, doi:10.1021/es060810w, 2006.

Paciga, A. L., Riipinen, I., and Pandis, S. N.: Effect of Ammonia on the Volatility of Organic Diacids, Environmental Science & Technology, 48(23), 13769-13775, doi:10.1021/es5037805, 2014.

Petters, M. D., and Kreidenweis, S. M.: A single parameter representation of hygroscopic growth and cloud condensation nucleus activity, Atmos. Chem. Phys., 7(8), 1961-1971, doi:10.5194/acp-7-1961-2007, 2007.

Pye, H. O. T., Murphy, B. N., Xu, L., Ng, N. L., Carlton, A. G., Guo, H., Weber, R., Vasilakos, P., Appel, K. W., Budisulistiorini, S. H., Surratt, J. D., Nenes, A., Hu, W., Jimenez, J. L., Isaacman-VanWertz, G., Misztal, P. K., and Goldstein, A. H.: On the implications of aerosol liquid water and phase separation for organic aerosol mass, Atmos. Chem. Phys., 17(1), 343-369, doi:10.5194/acp-17-343-2017, 2017.

Pye, H. O. T., Pinder, R. W., Piletic, I. R., Xie, Y., Capps, S. L., Lin, Y.-H., Surratt, J. D., Zhang, Z., Gold, A., Luecken, D. J., Hutzell, W. T., Jaoui, M., Offenberg, J. H., Kleindienst, T. E., Lewandowski, M., and Edney, E. O.: Epoxide Pathways Improve Model Predictions of Isoprene Markers and Reveal Key Role of Acidity in Aerosol Formation, Environmental Science & Technology, 47(19), 11056-11064, doi:10.1021/es402106h, 2013.

Pye, H. O. T., and Pouliot, G. A.: Modeling the Role of Alkanes, Polycyclic Aromatic Hydrocarbons, and Their Oligomers in Secondary Organic Aerosol Formation, Environmental Science & Technology, 46(11), 6041-6047, doi:10.1021/es300409w, 2012.

Pye, H. O. T., Zuend, A., Fry, J. L., Isaacman-VanWertz, G., Capps, S. L., Appel, K. W., Foroutan, H., Xu, L., Ng, N. L., and Goldstein, A. H.: Coupling of organic and inorganic aerosol systems and the effect on gas–particle partitioning in the southeastern US, Atmos. Chem. Phys., 18(1), 357-370, doi:10.5194/acp-18-357-2018, 2018.

Riedel, T. P., Lin, Y. H., Zhang, Z., Chu, K., Thornton, J. A., Vizuete, W., Gold, A., and Surratt, J. D.: Constraining condensed-phase formation kinetics of secondary organic aerosol components from isoprene epoxydiols, Atmos. Chem. Phys., 16(3), 1245-1254, doi:10.5194/acp-16-1245-2016, 2016.

Rollins, A. W., Kiendler-Scharr, A., Fry, J. L., Brauers, T., Brown, S. S., Dorn, H. P., Dubé, W. P., Fuchs, H., Mensah, A., Mentel, T. F., Rohrer, F., Tillmann, R., Wegener, R., Wooldridge, P. J., and Cohen, R. C.: Isoprene oxidation by nitrate radical: alkyl nitrate and secondary organic aerosol yields, Atmos. Chem. Phys., 9(18), 6685-6703, doi:10.5194/acp-9-6685-2009, 2009.

Sakulyanontvittaya, T., Guenther, A., Helmig, D., Milford, J., and Wiedinmyer, C.: Secondary Organic Aerosol from Sesquiterpene and Monoterpene Emissions in the United States, Environmental Science & Technology, 42(23), 8784-8790, doi:10.1021/es800817r, 2008.

Shiraiwa, M., Li, Y., Tsimpidi, A. P., Karydis, V. A., Berkemeier, T., Pandis, S. N., Lelieveld, J., Koop, T., and Pöschl, U.: Global distribution of particle phase state in atmospheric secondary organic aerosols, Nature Communications, 8(1), 15002, doi:10.1038/ncomms15002, 2017.

Simon, H., and Bhave, P. V.: Simulating the Degree of Oxidation in Atmospheric Organic Particles, Environmental Science & Technology, 46(1), 331-339, doi:10.1021/es202361w, 2012.

Zhang, Y., Nichman, L., Spencer, P., Jung, J. I., Lee, A., Heffernan, B. K., Gold, A., Zhang, Z., Chen, Y., Canagaratna, M. R., Jayne, J. T., Worsnop, D. R., Onasch, T. B., Surratt, J. D., Chandler, D., Davidovits, P., and Kolb, C. E.: The Cooling Rate- and Volatility-Dependent Glass-Forming Properties of Organic Aerosols Measured by Broadband Dielectric Spectroscopy, Environmental Science & Technology, 53(21), 12366-12378, doi:10.1021/acs.est.9b03317, 2019b.